Quantum magnetomechanics: Towards the ultrastrong coupling regime

E. Romero-Sánchez,[1] W. P. Bowen,[1] M. R. Vanner,[1,2] K. Xia,[3,4] and J. Twamley[3]

[1]*ARC Centre for Engineered Quantum Systems, School of Mathematics and Physics, The University of Queensland,*
Brisbane, Queensland 4072, Australia

[2]*Clarendon Laboratory, Department of Physics, University of Oxford, Oxford OX1 3PU, United Kingdom*

[3]*ARC Centre for Engineered Quantum Systems, Department of Physics and Astronomy, Macquarie University, NSW 2109, Australia*

[4]*National Laboratory of Solid State Microstructures, College of Engineering and Applied Sciences, Nanjing University,*
Nanjing 210093, China

In this paper we investigate a hybrid quantum system comprising a mechanical oscillator coupled via magnetic induced electromotive force to an *LC* resonator. We derive the Lagrangian and Hamiltonian for this system and find that the interaction can be described by a charge-momentum coupling with a strength that has a strong geometry dependence. We focus our study on a mechanical resonator with a thin-film magnetic coating which interacts with a nanofabricated planar coil. We determine that the coupling rate between these two systems can enter the strong and ultrastrong coupling regimes with experimentally feasible parameters. This magnetomechanical configuration allows for a range of applications including electromechanical state transfer and weak-force sensing.

I. INTRODUCTION

Coupling between electromagnetic and mechanical degrees of freedom is central to a number of quantum science experiments and enables the development of many quantum technologies. Mechanical oscillators can act as coherent interfaces between different electromagnetic fields [1,2] and are a promising tool for the development of future quantum technologies oriented to communications, memories, and metrology. Additionally, due to their relatively large mass, mechanical systems offer a promising route to perform fundamental tests of quantum physics [3–5]. A multitude of approaches in both opto- and electromechanics have been suggested and experimentally studied such as suspended mirrors forming an optical cavity with variable cavity length formed by microtoroids carrying whispering gallery modes [6], *LC* resonators with a mobile drum mode capacitor [7], the motion of superfluid [8,9], and nanophononic crystals [10].

The basic coupling in optomechanics and electromechanics is fundamentally similar but physically different. In both cases a mechanical displacement produces a shift in the resonance frequency of an electromagnetic resonator. In optomechanics optical resonators are formed by mobile elements that change the length of the cavity. In electromechanics, capacitors used in *LC* circuits are commonly formed by one mobile plate, so the resonance frequency is position dependent. Since the optomechanical coupling rate is related to the momentum transfer between the photon and a mechanical oscillator [11], it is usually small, such that reaching beyond the strong coupling regime is complicated. In recent literature, the term optomechanics is used to refer to both opto- and electromechanical systems [12]; we follow this convention along the rest of the text.

At the quantum level, many experimental control protocols require quantum-coherent exchange of excitations between the light and mechanical systems [13], which is possible when the optomechanical interaction is faster than the dissipation of the light and mechanics, known as strong coupling condition. Significant progress has been made in a variety of architectures that enables this strong coupling to be observed [14]. Strongly coupled systems have been used, for instance, to cool down the state of motion of mechanical oscillators to their ground state [15] and the preparation of entangled states of motion of a macroscopic mechanical oscillator [7]. The magnitude of the coupling rate defines two other main regimes that remain unexplored in optomechanics. The first one, referred to as ultrastrong coupling regime, is accessible when the coupling rate is a considerable fraction of the resonance frequency [16–18]. In optomechanical systems, the ultrastrong coupling regime has been proposed to exhibit novel physics at the quantum level [19,20].

Approaches that explore mechanical oscillators coupled to electric circuits through magnetic interactions have been referred to as *magnetomechanics* and have been little explored compared to electromechanics [21]. Quantum magnetomechanics explores different techniques to prepare and control quantum states of motion of a mechanical oscillator using magnetic interactions. Several approaches to quantum magnetomechanics have been proposed and include magnetically levitated mechanical oscillators with the aim of reduce decoherence [22,23] and coupling the motion of a mechanical oscillator to a superconducting circuit [24]. The applications of quantum magnetomechanics can be expanded to systems with intrinsic magnetic properties such as electric circuits, superconducting qubits [25], or spin qubits [26].

In this paper we reexamine an electromechanical scheme, dating back as far as 1980 [3], that utilizes inductive coupling, placing it on a solid theoretical formulation by deriving the Lagrangian and the associated Hamiltonian. We further explore experimental regimes that may be achieved using modern
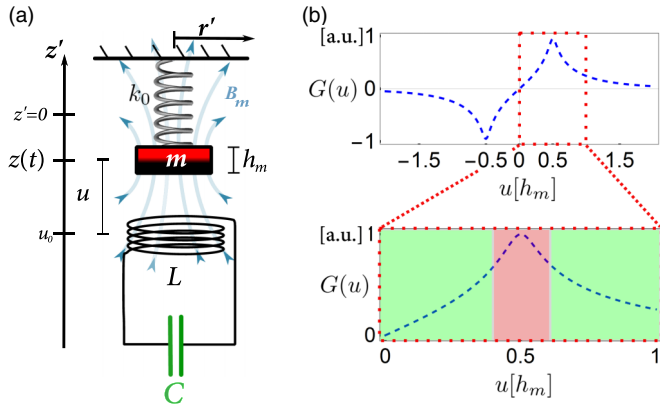
FIG. 1. (a) Simplified scheme of the magnetomechanical system described in cylindrical coordinates z' and r'. A cylindrical magnet of mass m and thickness h_m attached to a spring of stiffness k_0 forms a mechanical oscillator. The mechanical oscillator is inductively coupled to an LC resonator. The magnet produces a magnetic field $\mathbf{B}_m$ that induces a flux in the inductor L placed at $z' = u_0$, which is connected to a capacitor C. The equilibrium position of the center of mass of the magnet is $z' = u_0$ and it displaces $z(t)$ around it. (b) Coupling rate $G(u)$ [a.u.] normalized to the maximum, which is proportional to the Faraday flux force on the magnet, as a function of the separation between the magnet and the coil u. The region where the linear (green) interaction is presented on both sides and where the dominant interaction is quadratic (red) is in the center.

fabrication techniques. The magnetomechanical system that we study is composed of a mechanical oscillator coupled magnetically to an LC resonator as shown in Fig. 1(a). In contrast to optomechanics, where the mediating force is due to the radiation pressure, in our magnetomechanical system the mediating force is the Lorentz force. Using micro/nanofabricated designs which are experimentally achievable we find that strong and ultrastrong coupling are attainable.

An outline of the paper is as follows. In Sec. II we determine the Lagrangian of the coupled mechanical-LC system and then derive the quantized Hamiltonian. The quantum Hamiltonian exhibits either an adjustable linear or quadratic coupling (Sec. III). In the linear coupling regime IV we find that the LC circuit couples to the mechanical momentum identical to the velocity sensor studied in [3]. We explore the linear system in the strong coupling regime in Sec. IV A, and the generalized dynamics beyond the strong coupling in Sec. IV B. We find the energy spectrum and the eigenstates of the magnetomechanical system and estimate the occupation for its ground state, finding signs of entanglement between the mechanics and the electronics in Sec. IV B 2. We study the system in the presence of decoherence and analyze some of the spectral properties of the mechanical system in the presence of the inductive coupling in Sec. V. Properties of the proposed experimental device are discussed in Sec. VI where we consider an implementation with high Q mechanical oscillators and a superconducting LC resonator. The linear dependence of the Hamiltonian on the mechanical momentum also suggests that the Hamiltonian is not invariant under the reversal of time, i.e., $t \to -t$, and thus breaks time-reversal symmetry and we discuss this in the Appendix.

II. SEMICLASSICAL PICTURE

We define a cylindrical coordinate system (r', z'), where we consider a small cylindrical magnet with magnetization M and vector $\mathbf{M} = M\mathbf{e}_{z'}$. The magnet generates a magnetic field $\mathbf{B}_m(z', r') = B_z\mathbf{e}_{z'} + B_r\mathbf{e}_{r'}$ [27]. In Fig. 1(a) we represent a scheme for the magnet's position of the center of mass $z(t)$ placed at its equilibrium position $z' = 0$. The magnet, with effective mass m, is attached to a spring with spring constant k_0, forming a mechanical oscillator which resonates at the frequency $\omega_m = \sqrt{k_0/m}$. The equation of motion for the center of mass of the magnet is given by $m[\ddot{z}(t) + \Gamma_m\dot{z}(t) + \omega_m^2 z(t)] = F_{ext}(t)$, where Γ_m represents the mechanical damping rate and $F_{ext}(z,t)$ is an arbitrary external driving force.

Here we use a planar electric coil with inductance L placed vertically below the magnet at $z' = u_0$ and connected to a two plate capacitor C. This combination of capacitor and inductor creates a cavity with resonance frequency centered at $\omega_e = 1/\sqrt{LC}$. The equation of motion for an LC resonator that is driven with an arbitrary external voltage $V_{ext}(t)$ is given by $L[\ddot{q}(t) + \Gamma_e\dot{q}(t) + \omega_e^2 q(t)] = V_{ext}(t)$, where $\Gamma_e = R/L$ is the dissipation rate and R is the resistance of the entire circuit.

The planar inductor follows a geometrical path in three dimensions, which we define via a vector path $\mathbf{S}$ whose transversal area element $d\mathbf{a} = da\,\mathbf{e}_{z'}$ is normal to the plane where the inductor lays. The magnetic flux crossing the area enclosed by the inductor is $\Phi_B = \int \mathbf{B}_m(u) \cdot d\mathbf{a}$, where $u = z(t) - u_0$ represents the relative vertical separation between the magnet and the coil. Here we treat the Lorentz force $F_L(t)$ as the dominant force acting on the magnet so $F_{ext}(t) = F_L(t)$. and the electromotive force (EMF) $\mathcal{E}(t)$ as the main source of voltage $V_{ext}(t) = \mathcal{E}(t)$. In Sec. V we discuss the case where the system is thermally driven.

As the magnet displaces along z', it fluctuates around an equilibrium position $z' = u_0$. The mechanical vertical motion creates an ac magnetic field which couples the LC circuit-mechanical system via mutual inductance. The change in position induces then a change in flux generating an EMF in the electric circuit $\mathcal{E}(t) = -\frac{d\Phi_B}{dt}$. The displacement is restricted to the z' axis and it is parallel to the area component $\mathbf{a}$; using the expression for the time derivative of flux [28], the EMF can be reexpressed in terms of the magnetic field

$$\mathcal{E}(t) = -\dot{z}(t) \oint_{coil} \mathbf{e}_{z'} \cdot (\mathbf{B}_m(u) \times d\mathbf{S}). \tag{1}$$

The induced $\mathcal{E}(t)$ produces an small current in the LC circuit, and the inductor carrying the current generates a magnetic field which interacts with the magnetic field of the permanent magnet exerting a Lorentz force $\mathbf{F}_L(t)$ between the mechanical oscillator and the LC circuit

$$\mathbf{F}_L(t) = -\dot{q}(t) \oint_{coil} \mathbf{B}_m(u) \times d\mathbf{S}. \tag{2}$$

The Lorentz force $\mathbf{F}_L(t) = F_z(t)\mathbf{e}_{z'} + F_r(t)\mathbf{e}_{r'}$ has a radial component $F_r(t)\mathbf{e}_{r'}$ which points radially inwards; therefore, around a closed loop $\langle F_r(t)\rangle \approx 0$. The simplified expression for the Lorentz force is the contribution of the vertical component $F_z(t) = -\dot{q}(t)(\oint_{coil} \mathbf{B}_m(u) \times d\mathbf{S}) \cdot \mathbf{e}_{z'}$. The effect of this force acting on the mechanical oscillator produces a modification of the stiffness of the mechanical spring constant and we denote

it as the Lorentz spring constant k_L. By altering the current in the inductor this spring constant can be modified allowing one to electrically tune the mechanical resonance frequency. From Eq. (1) and Eq. (2) we define

$$G(u) = \oint_{\text{coil}} [\mathbf{B}_{\text{m}}(u) \times d\mathbf{S}] \cdot \mathbf{e}_{z'}, \qquad (3)$$

as the magnetomechanical coupling term $G \propto M$, which couples the mechanical and electrical interactions through a magnetic interaction.

The magnetomechanical coupling rate $G(u)$ is a function of the relative separation between the magnet and the coil $u = z(t) - u_0$. In Fig. 1(b) we plot the coupling rate $G(u)$ as a function of u, which can be freely controlled in an experiment. We set the initial equilibrium separation u_0 with $u_0/h_{\text{m}} \in [0,1]$, where h_{m} is the thickness of the magnet [Fig. 1(a)]. The small displacement of the magnet around u_0 allows us to expand $G(u) \rightarrow G(u_0 + z(t))$ as a function of z, the canonical coordinate of the center of mass mechanical motion. For small displacements around u_0, we define the linear coupling rate $G_0 = G(u_0)$ and expand $G(z) \approx G_0 + G_j z^j$ where the generalized expression $G_j = \partial^j G(z)/\partial z^j|_{z'=u_0}$ and $j = 1,2$. The choice of u_0 will define two different regions that correspond to different dominant nonlinear terms of $G(z)$. The first region is shown in color green in Fig. 1(b) (bottom); the dominant interaction in this region is defined by the first order term ($j = 1$). The second region is illustrated as a red colored area in Fig. 1(b) and the dominant nonlinear term is the second order one ($j = 2$). The following analysis is equivalent for $j = 1,2$. For the sake of simplicity, we will focus on the interaction up to first order ($j = 1$).

Now we consider that the two oscillators are driven externally, with the force Eq. (2) for the mechanics and the voltage Eq. (1) for the electronics. The dynamics of the coupled system is then described by the set of coupled equations of motion:

$$m[\ddot{z}(t) + \Gamma_{\text{m}}\dot{z}(t) + \omega_{\text{m}}^2 z(t)] = -\dot{q}(t)G(z),$$
$$L[\ddot{q}(t) + \Gamma_{\text{e}}\dot{q}(t) + \omega_{\text{e}}^2 q(t)] = \dot{z}(t)G(z). \qquad (4)$$

Clearly, the magnetomechanical system is coupled through $G(z)$. Keeping in mind that our goal is to obtain a quantum description of the system, we require the calculation of the lossless magnetomechanical Lagrangian $\mathcal{L}$ from which we can derive the equations of motion (4). We find that this lossless Lagrangian is

$$\mathcal{L}(z,q,\dot{z},\dot{q}) = \left(\frac{m}{2}\dot{z}^2 - \frac{m}{2}\omega_{\text{m}}^2 z^2\right) + \left(\frac{L}{2}\dot{q}^2 - \frac{L}{2}\omega_{\text{e}}^2 q^2\right)$$
$$+ G(z)z\dot{q} + \frac{d}{dt}[q\,\varphi(z)], \qquad (5)$$

where the first two terms in Eq. (5) describe the two oscillators. The third term in Eq. (5) is the magnetomechanical coupling rate between the motional displacement and the small currents $\dot{q}$. The last term is a total gauge derivative; although the gauge $\varphi(z)$ is a free parameter and can be arbitrarily chosen, it is common that some specific physical conditions influence the choice of gauge. The fourth term is easily expanded as $\partial_t[q\,\varphi(z)] = q\dot{z}\nabla\varphi(z) + \varphi(z)\dot{q}$ (∂_t is the time derivative operator) leaves the coupled equations of motion (4) invariant.

The canonical flux ϕ and the canonical momentum p are obtained through the equations

$$\frac{\partial \mathcal{L}}{\partial \dot{q}} = \phi = L\dot{q} + z\,G(z) + \varphi(z),$$
$$\frac{\partial \mathcal{L}}{\partial \dot{z}} = p = m\dot{z} + q\,\nabla\varphi(z). \qquad (6)$$

As we observe, the canonical momentum p is a gauge dependent quantity, in our very particular case we chose $\varphi(z) = -G_0 z$, that simplifies the ultimate form of the Hamiltonian plus recovers the external capacitance in the readout circuit $C_k = m/G_0^2$ due to the coupling rate G_0 [3]. Applying the Legendre transformation $\mathcal{H}(z,q,p,\phi) = \dot{z}p + \dot{q}\phi - \mathcal{L}$ to Eq. (5), one obtains the canonical momentum and canonical flux of the oscillators

$$p = m\dot{z} - G_0\,q, \quad \phi = L\dot{q} + z\,G(z). \qquad (7)$$

The canonical momentum p of the coupled system includes the kinetic momentum $m\dot{z}$ and the momentum in the field $-G_0 q$. The canonical flux ϕ involves the current $L\dot{q}$ and an induction term $G_1 z$. Therefore, the total classical Hamiltonian is derived from the Lagrangian through the Legendre transformation and it is given by

$$\mathcal{H} = \left(\frac{p^2}{2m} + \omega_{\text{m}}^2 \frac{mz^2}{2}\right) + \left[\frac{\phi^2}{2L} + \left(\omega_{\text{e}}^2 + \frac{G_0^2}{mL}\right)\frac{Lq^2}{2}\right]$$
$$+ \left(\frac{G_0}{m}\,pq + \frac{G_1}{L}\phi z^2\right). \qquad (8)$$

We have so far found the Hamiltonian (8); in order to quantize it, it is required to analyze the magnetomechanical single photon-phonon interaction. We define the effective linear coupling g_0 in terms of the zero point fluctuation of the electric charge $q_{\text{ZPF}} = \sqrt{\hbar/(2L\omega_{\text{e}})}$ and mechanical momentum $p_{\text{ZPF}} = \sqrt{\hbar\omega_{\text{m}}m/2}$ such that

$$\frac{\hbar g_0}{2} \equiv G_0\,q_{\text{ZPF}}\frac{p_{\text{ZPF}}}{m}, \quad \frac{\hbar g_1}{2} \equiv G_1\,z_{\text{ZPF}}^2\frac{\phi_{\text{ZPF}}}{L}, \qquad (9)$$

where we also defined the nonlinear coupling g_1 in terms of the zero point motion $z_{\text{ZPF}} = \sqrt{\hbar/(2m\omega_{\text{m}})}$ and zero point fluctuation of the electrical flux $\phi_{\text{ZPF}} = \sqrt{\hbar L\omega_{\text{e}}/2}$. Within this paper, we mostly study the regime near to resonance in which the single photon-phonon effective linear coupling is simplified as

$$g_0 = \frac{G_0}{\sqrt{Lm}}. \qquad (10)$$

The linear coupling is commonly characterized using spectroscopic techniques, which we discuss in Sec. V B. The geometrical dependence of the linear coupling g_0 is described in Sec. VI.

III. QUANTUM DYNAMICS

In this section we explore the quantum magnetomechanical Hamiltonian and some potential applications of a quantum system of these physical characteristics. Following the standard process in opto- and electromechanics [29], we quantize the classical Hamiltonian (8) with the standard commutation relations $[\hat{q},\hat{p}] = [\hat{z},\hat{\phi}] = [\hat{z},\hat{q}] = [\hat{p},\hat{\phi}] =$

0 and $[\hat{q},\hat{\phi}] = [\hat{z},\hat{p}] = i\hbar$. The quantum magnetomechanical Hamiltonian $\hat{H}_m$ is given by

$$\hat{H}_m = \left(\frac{\hat{\phi}^2}{2L} + (\omega_e^2 + g_0^2)\frac{L\hat{q}^2}{2}\right) + \left(\frac{\hat{p}^2}{2m} + \Omega_m(\hat{\phi})^2\frac{m\hat{z}^2}{2}\right)$$
$$+ g_0\sqrt{\frac{L}{m}}\hat{p}\hat{q}, \tag{11}$$

where the mechanical frequency is modulated by the flux in the LC circuit as

$$\Omega_m^2(\hat{\phi}) = \omega_m^2 - \frac{2g_1}{\sqrt{Lm}}\hat{\phi}. \tag{12}$$

The Lorentz force exerted between the permanent magnet and the field generated by the current induces the modulation of the mechanical frequency Ω_m. The effect is known as Lorentz spring constant $k_L = -2g_1\sqrt{m/L}$ as a result of the modification of the total stiffness $k = k_0 + k_L$ of the mechanical oscillator.

The magnetomechanical Hamiltonian clearly allows one to perform mechanical frequency modulation through the Lorentz force:

$$\hat{F}_L = -\frac{\partial \hat{H}_{int}}{\partial \hat{z}} = 2g_1\sqrt{\frac{m}{L}}\hat{z}\hat{\phi}. \tag{13}$$

One of the applications of the Lorentz force at the mesoscale is the implementation of its backaction to cool down the mechanical motion of mechanical oscillators [30]. The nonlinear properties of the Hamiltonian in Eq. (11) represent an introduction for the nonlinear dynamics of mechanical systems [31]. The second order nonlinear interaction ($\hat{\phi}\hat{z}^2$) of Eq. (15) induces an x-squared-type nonlinearity, allowing one to produce mechanical squeezing [32], mechanical amplification [33], mechanical entanglement [34], or cooling through mechanical frequency modulation [35].

In the general magnetomechanical interaction, we look at two different regimes of interest depending on the strength of the coupling rates g_0 and g_1. Since, in general $|g_0| \gg |g_1|$, the terms involving g_1^2 are usually negligible, we may write the magnetomechanical Hamiltonian as a sum of linear and nonlinear terms, i.e., $\hat{H}_m = \hat{H}_L + \hat{H}_{NL}$, where

$$\hat{H}_L = \frac{\hat{\phi}^2}{2L} + (\omega_e^2 + g_0^2)\frac{L\hat{q}^2}{2} + \frac{\hat{p}^2}{2m} + \omega_m^2\frac{m\hat{z}^2}{2} + g_0\sqrt{\frac{L}{m}}\hat{p}\hat{q} \tag{14}$$

and

$$\hat{H}_{NL} \approx g_1\sqrt{\frac{m}{L}}\hat{z}^2\hat{\phi}. \tag{15}$$

With H_L alone we recover a scheme proposed for quantum nondemolition measurements and velocity sensing [3].

In the optomechanics community, the Hamiltonian is typically expressed in the boson representation. In order to facilitate the comparison between magnetomechanics and optomechanics, here we reexpress our magnetomechanical Hamiltonian (11) in the boson operators representation:

$$\hat{H}_m = \hbar\omega_e\hat{a}^\dagger\hat{a} + \hbar\Omega_m(\hat{\phi})\hat{b}^\dagger\hat{b} + i\frac{\hbar g_0}{2}(\hat{a}^\dagger + \hat{a})(\hat{b} - \hat{b}^\dagger)$$
$$+ \frac{\hbar g_0^2}{4\omega_e}(\hat{a} + \hat{a}^\dagger)^2. \tag{16}$$

We introduce the boson creation $\hat{a}^\dagger$ ($\hat{b}^\dagger$) and the annihilation $\hat{a}$ ($\hat{b}$) operators for the electromagnetic (acoustic) field. The boson operators are defined by the relations $\hat{q} = q_{ZPF}(\hat{a} + \hat{a}^\dagger)$, $\hat{\phi} = i\phi_{ZPF}(\hat{a}^\dagger - \hat{a})$, $\hat{z} = z_{ZPF}(\hat{b} + \hat{b}^\dagger)$, and $\hat{p} = ip_{ZPF}(\hat{b}^\dagger - \hat{b})$. The boson operators act on the eigenstates of the electromagnetic (acoustic) field mode $|n_e\rangle$ ($|n_m\rangle$) following the standard raising $\hat{a}^\dagger|n_e\rangle = \sqrt{n_e + 1}|n_e + 1\rangle$ ($\hat{b}^\dagger|n_m\rangle = \sqrt{n_m + 1}|n_m + 1\rangle$) and lowering $\hat{a}|n_e\rangle = \sqrt{n_e - 1}|n_e - 1\rangle$ ($\hat{b}|n_b\rangle = \sqrt{n_m - 1}|n_m - 1\rangle$) relations. The eigenvector basis for the magnetomechanical states is described by $|n_e,n_m\rangle = |n_e\rangle \otimes |n_m\rangle$.

IV. LINEAR QUANTUM MAGNETOMECHANICS

In this section, we focus our study on the linear magnetomechanical Hamiltonian $\hat{H}_L$, where $g_0 \gg g_1$. This raises a dominant linear interaction defined by the charge-momentum coupling $\hat{q}\hat{p}$. In regular optomechanics, the interaction is commonly described by a linearized model with a bilinear position-position coupling [36]. In the magnetomechanical linear interaction picture we explore two different regimes: the so-called strong coupling regime and ultrastrong coupling regime. Charge-momentum coupling remains little explored, and to the best of our knowledge there are no proposals demonstrating that ultrastrong coupling for mechanical systems can be achieved in this fashion. We also note that our magnetomechanical system breaks the time-reversal symmetry (Appendix).

A. Strong coupling regime

In the magnetomechanical strong coupling regime the interaction between the mechanics and the electronics is faster than the decoherence for each individual resonator $g_0^{-1} < \Gamma_m^{-1}, \Gamma_e^{-1}$. In the strong coupling regime $g_0 \ll \omega_m, \omega_e$ and the term $g_0^2/\omega_e \ll g_0$. The elements in (14) in the boson basis with terms proportional to g_0^2/ω_e are negligible and the simplified Hamiltonian in the strong coupling regime is

$$\hat{H}_{SC} = \hbar\omega_e\hat{a}^\dagger\hat{a} + \hbar\omega_m\hat{b}^\dagger\hat{b} + i\frac{\hbar g_0}{2}(\hat{a}^\dagger + \hat{a})(\hat{b} - \hat{b}^\dagger), \tag{17}$$

which is easily diagonalized as the sum of two normal modes $\hat{H}_{SC} = \hbar\omega_{SC+}\hat{c}_+^\dagger\hat{c}_+ + \hbar\omega_{SC-}\hat{c}_-^\dagger\hat{c}_-$. The normal modes $\hat{c}_\pm$ are a hybridized mode that contains phonon and photon modes. The energy levels for the hybrid system are

$$E_{SC\pm} = \frac{\hbar}{\sqrt{2}}\left(\omega_m^2 + \omega_e^2 \pm \sqrt{4g_0^2\omega_e^2 + (\omega_m^2 - \omega_e^2)^2}\right)^{1/2}. \tag{18}$$

The spectrum for the first eight eigenvalues are shown in red dashed lines in Fig. 2(a) as a function of g_0/ω_m for values that lay within the strong coupling regime ($\Gamma_m/\omega_m < g_0/\omega_m \leqslant 0.1$); in blue are the values obtained for the general solution discussed in the next section. In this regime we observe a very typical linear dependence and good agreement between the general and strong coupling approximation.

The Hamiltonian Eq. (17) shows that, in the strong coupling regime, the magnetomechanical linear system allows one to perform linear operations available in optomechanics such as state swap between the mechanics and the electronics, cooling or heating of the mechanical oscillator through a
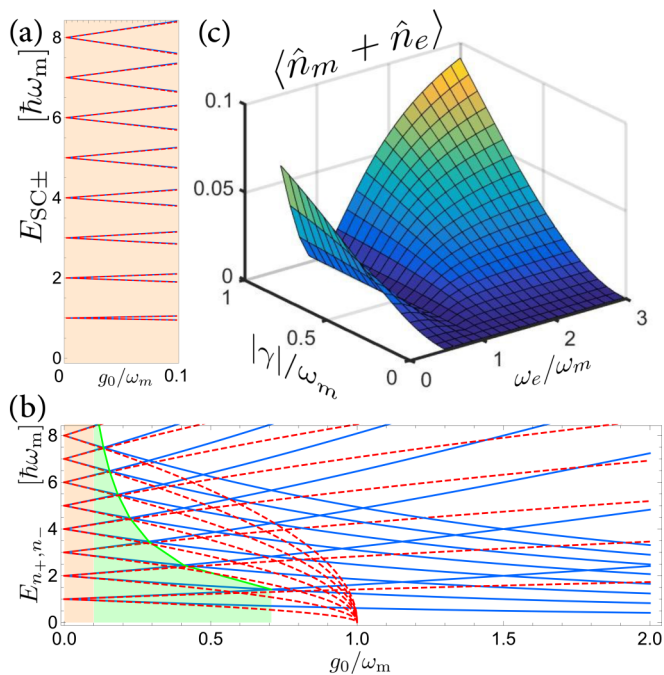
FIG. 2. In blue lines, the generalized spectrum and in red dashed lines the approximation for the spectra in the strong coupling regime. (a) Energy spectra of the magnetomechanical system within the strong coupling regime $g_0/\omega_{\rm m}$. (b) Energy spectra of the magnetomechanical system in two different perturbative regimes, strong coupling (orange background $0 \leqslant g_0/\omega_{\rm m} \leqslant 0.1$) and ultrastrong coupling (green background $0.1 \leqslant g_0/\omega_{\rm m} \leqslant 1/\sqrt{2}$). The green line represents the Juddian points that delimit the perturbative ultrastrong coupling regime. The spectra (a) and (b) were calculated considering in resonance a resonant system $\omega_{\rm e} = \omega_{\rm m}$. (c) Expectation value of the total excitation number populating the ground state $\langle n_{\rm e} + n_{\rm m} \rangle$. The calculation was performed using a truncation of 15 Fock states.

magnetomechanical protocol, and squeezing of the mechanical mode or implementation of *quantum nondemolition* protocols. The terms $\propto (\hat{a}^\dagger \hat{b} - \hat{a}\hat{b}^\dagger)$ in the Hamiltonian Eq. (17) represent the energy exchange between electronic and mechanical mode, commonly known as beam splitter interaction and crucial for state transfer protocols. Meanwhile, the terms $\propto (\hat{a}\hat{b} - \hat{a}^\dagger \hat{b}^\dagger)$ are simultaneous excitations of the mechanical and electromagnetic field, known as two mode squeezing interaction [37,38]. The magnetomechanical system in the linear regime reveals an interface to implement hybrid mechanical systems with strong interactions.

In Sec. V we expand the discussion of spectral properties and suitable measurements for the strong magnetomechanical coupling regime.

B. Perturbative ultrastrong coupling regime

The magnetomechanical system offers a new platform for the exploration of regimes beyond the strong coupling, where relevant phenomena have been described in modern literature [20,39,40]. The ultrastrong coupling regime has been predominantly explored with electronic circuits [39,41,42]. Our system opens the possibility for mechanical systems to reach this developing regime.
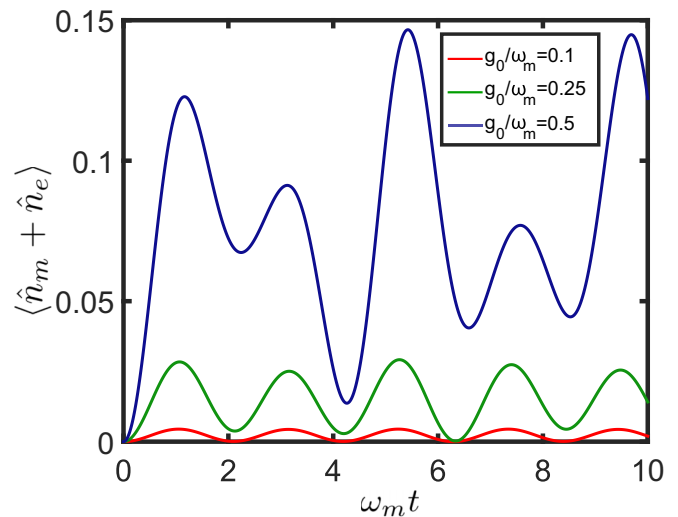

FIG. 3. Examining the dependence of the validity of the RWA on the coupling strength $g_0/\omega_{\rm m}$. We consider the linear system with $\omega_{\rm e}/\omega_{\rm m} = 2$ and plot the time dependence of the total occupation $n_T(t)$, under the full Hamiltonian for increasing coupling strengths $g_0/\omega_{\rm m} = (0.1, 0.25, 0.5)$ for the initially unoccupied state $|\psi_i\rangle = |n_{\rm e}, n_{\rm m}\rangle = |0,0\rangle$. For $g_0/\omega_{\rm m} = 0$ the evolution under the full Hamiltonian agrees perfectly with with $n_T(t) = 0$. Under the RWA $n_T(t) = 0$ for all times and all coupling strengths. For $0 < g_0/\omega_{\rm m} \leqslant 0.1$ (red) the evolution exhibits a periodic oscillation with very small amplitude $n_T(t) > 0$. However, the full dynamics shows that the total occupation increases substantially for larger coupling strengths indicating that the RWA breaks under ultrastrong coupling in our model (green and blue).

As has been demonstrated [18], the transition between coupling regimes is smooth as a function of $g_0/\omega_{\rm m}$ and can be identified through the spectral properties of the system [18,43], but it is also common to characterize the transition from the strong coupling regime to ultrastrong coupling analyzing the rotating wave approximation (RWA). In our system we look at the evolution of the initial state $|\psi_i\rangle = |n_{\rm e}, n_{\rm m}\rangle = |0,0\rangle$, which has no initial excitations in either the electrical or mechanical oscillators under the Hamiltonian (14), for the case $\omega_{\rm e}/\omega_{\rm m} = 2$, with an optomechanical coupling initiated at $t = 0$ and with strength $g_0/\omega_{\rm m} = 0, 0.1, 0.25, 0.5$. We compare the mean total occupation $n_T(t) \equiv \langle \hat{n}_{\rm e} + \hat{n}_{\rm m} \rangle(t)$, under the full linear Hamiltonian and with the RWA approximation which involves dropping the fast rotating terms in the interaction term $\sim \hat{p}\hat{q} \sim (\hat{a}^\dagger \hat{b} - \hat{a}\hat{b}^\dagger)$. For $g_0 = 0$, $|\psi_i\rangle$ is the ground state with no excitations and evolution by the full dynamics and truncated RWA agree. This is no longer the case when $0.1 \geqslant g_0/\omega_{\rm m} > 0$; as we can see in Fig. 3 the evolution of $n_T(t) > 0$ is periodic oscillating between a maximum value and a periodic minimum close to zero.

For $g_0/\omega_{\rm m} > 0.1$ the maximum of $n_T(t)$ increases and the dynamics becomes less periodic with minimum only approaching to zero after several oscillation cycles. We can define the boundary between the strong and ultrastrong coupling regimes at a given value $g_0/\omega_{\rm m}$ at which the dynamics starts changing, the periodicity of $n_T(t)$ in the strong coupling regime starts to break, and the amplitude of $n_T(t)$ starts to increase. This boundary is not an exact numerical value but according to our

calculations the dynamics starts to change for $g_0/\omega_{\rm m} \sim 0.1$, which agrees with the typical value considered in the literature.

The treatment for $\hat{H}_L$ in the ultrastrong coupling becomes a more complicated task when terms in the Hamiltonian are not negligible any more. Here we consider a lossless environment $\Gamma_{\rm m,e} = 0$ and find a general diagonalization for $\hat{H}_L$ and the construction of the eigenstates of the magnetomechanical system and spectral properties.

1. Eigenstates of the magnetomechanical system

To construct the eigenstates of the magnetomechanical system beyond the strong coupling approximation is needed to diagonalize the Hamiltonian $\hat{H}_L$ into its normal modes. The normal modes are given by $\hat{H}_{\rm NM} = \hat{U} \hat{H}_L \hat{U}^\dagger$, which is diagonal and has normal mode frequencies $\omega_\pm$. The unitary transformation $\hat{U}$ is a two mode squeezing operator $\hat{U} = \exp\{i\beta(e^{-\gamma} \hat{p}\hat{\phi} - e^\gamma \hat{z}\hat{q})\}$ following [44] with complex squeezing parameter $e^\gamma = i\, Lm\, \omega_{\rm m}\sqrt{\omega_{\rm m}\omega_{\rm e}}$. The diagonalized linear lossless Hamiltonian $\hat{H}_{\rm NM}$ is expressed in the normal mode basis as

$$\hat{H}_{\rm NM} = \frac{\omega_-^2}{2}(\hat{X}_-^2 + \hat{P}_-^2) + \frac{\omega_+^2}{2}(\hat{X}_+^2 + \hat{P}_+^2), \qquad (19)$$

where the eigenfrequencies are given by

$$\omega_\pm^2 = \tfrac{1}{2}\big(\omega_{\rm m}^2 + \omega_{\rm e}^2 + g_0^2\big)$$
$$\pm \tfrac{1}{4}\sqrt{4g_0^2\big(\omega_{\rm e}^2 + g_0^2\big) + \big(\omega_{\rm m}^2 - \omega_{\rm e}^2 - g_0^2\big)^2}. \qquad (20)$$

The dimensionless quadratures in the normal mode basis for position $\hat{X}_\pm$ and momentum $\hat{P}_\pm$ follow the standard commutation relations $[\hat{X}_\pm, \hat{P}_\pm] = i$ and each one of the quadratures is defined as

$$\hat{X}_+ = \frac{1}{\sqrt{2}q_{\rm ZPF}}(\hat{q}\,\cosh\beta + e^{-\gamma}\hat{p}\,\sinh\beta),$$

$$\hat{P}_+ = \frac{1}{\sqrt{2}\phi_{\rm ZPF}}(\hat{\phi}\,\cosh\beta + e^\gamma\hat{z}\,\sinh\beta),$$

$$\qquad\qquad (21)$$

$$\hat{X}_- = \frac{1}{\sqrt{2}z_{\rm ZPF}}(\hat{z}\,\cosh\beta + e^{-\gamma}\hat{\phi}\,\sinh\beta),$$

$$\hat{P}_- = \frac{1}{\sqrt{2}p_{\rm ZPF}}(\hat{p}\,\cosh\beta + e^\gamma\hat{q}\,\sinh\beta),$$

where $i\,\tanh(2\beta) = \frac{2g_0\omega_{\rm m}}{g_0^2 + \omega_{\rm e}^2 - \omega_{\rm m}^2}$.

As a matter of completeness, we introduce the boson creation and annihilation operators for the $\pm$ modes, defined as

$$\hat{a}_+ = \frac{1}{\sqrt{2}}(\hat{X}_+ + i\hat{P}_+), \quad \hat{a}_+^\dagger = \frac{1}{\sqrt{2}}(\hat{X}_+ - i\hat{P}_+),$$

$$\hat{a}_- = \frac{1}{\sqrt{2}}(\hat{X}_- + i\hat{P}_-), \quad \hat{a}_-^\dagger = \frac{1}{\sqrt{2}}(\hat{X}_- - i\hat{P}_-). \quad (22)$$

With the boson operators Eq. (22) defined, it is straightforward to determine the eigenstates of the magnetomechanical system in the linear regime, which are

$$|n_+, n_-\rangle = \frac{1}{\sqrt{n_+! n_-!}}(\hat{a}_+^\dagger)^{n_+}(\hat{a}_-^\dagger)^{n_-}|0,0\rangle, \qquad (23)$$

with the raising operators $\hat{a}_\pm$ acting on the vacuum state $|0,0\rangle$. Some of the relevant properties of the boson operators Eq. (22) are the standard commutation relations $[\hat{a}_+, \hat{a}_+^\dagger] =$

1 and $[\hat{a}_-, \hat{a}_-^\dagger] = 1$. Similarly, the number operator for the bosonic modes are $\hat{n}_+ \equiv \hat{a}_+^\dagger \hat{a}_+$ and $\hat{n}_- \equiv \hat{a}_-^\dagger \hat{a}_-$, with expectation values $n_\pm = \langle \hat{n}_\pm \rangle$. Once the system has been expressed in the boson operator representation, it is clear that, neglecting the vacuum energy, the system has the following energy spectrum:

$$E_{n_+, n_-} = \hbar\omega_+ n_+ + \hbar\omega_- n_-. \qquad (24)$$

The energy spectrum Eq. (24) as a function of $g_0/\omega_{\rm m}$ with its first eight eigenvalues is shown in Fig. 2(b) in continuum blue lines. In red dashed lines is shown the spectrum Eq. (18) which corresponds to the strong coupling regime approximation. It is clear that for small values of $0 \leqslant g_0/\omega_{\rm m} \leqslant 0.1$ the strong coupling spectrum of Fig. 2(a) accurately describes the energy levels of the system as the red dashed lines mostly overlap the blue lines. A modern quantitative definition for classification of coupling regimes according to spectral properties [18] suggests that the so-called ultrastrong coupling regime can be separated into perturbative and nonperturbative ultrastrong coupling regimes, where the perturbative ultrastrong coupling regime is defined as the region where $g_0/\omega_{\rm m} \leqslant J_n$, where J_n are the first Juddian points of the spectra. We calculated the Juddian points for the spectra of the magnetomechanical system

$$J_n = \frac{1}{\sqrt{n_- + n_-^2}}, \qquad (25)$$

which are shown in Fig. 2(b) as black crosses. According to Rossatto *et al.* [18], the perturbative ultrastrong coupling regime will be delimited by the first Juddian point for $n_- = 1$. The magnetomechanical perturbative ultrastrong coupling regime is then defined for coupling within $g_0/\omega_{\rm m} \leqslant \frac{1}{\sqrt{2}}$. The coupling rate g_0 can be experimentally measured directly from the electrical resonance frequency shift $\omega_{\rm e} \to \Omega_{\rm e}$, with $\Omega_{\rm e} = \sqrt{\omega_{\rm e}^2 + g_0^2}$. If the value of the frequency shift is negligible, the energy spectrum (18) defines the energy levels.

2. Entangled ground state

As we defined the diagonalized Hamiltonian in the normal mode basis Eq. (19), when they act on a on an eigenstate $|n_+, n_-\rangle$, we obtain $\hat{H}_{\rm NM}|n_+, n_-\rangle = E_{n_+, n_-}|n_+, n_-\rangle$. We can transform these eigenstates back to the laboratory frame using the unitary $\hat{U}^\dagger$, and denote them as $\overline{|n_+, n_-\rangle} \equiv \hat{U}^\dagger |n_+, n_-\rangle$. We note that in the laboratory basis such eigenstates may be entangled. To see this we look at the expectation values for the standard occupations for the number operators for the electric and mechanical excitations $\hat{n}_{\rm e} = \hat{a}^\dagger \hat{a}$, $\hat{n}_{\rm m} = \hat{b}^\dagger \hat{b}$, in this laboratory frame. In particular, we compute the sum $\langle \hat{n}_{\rm m} + \hat{n}_{\rm e} \rangle \equiv \overline{\langle 0,0|}\hat{n}_{\rm e}\overline{|0,0\rangle} + \overline{\langle 0,0|}\hat{n}_{\rm m}\overline{|0,0\rangle}$ (with a Fock truncation of 15), and in Fig. 2(c) we plot this sum as a function of $\omega_{\rm e}/\omega_{\rm m}$ and $\gamma/\omega_{\rm m}$. We see that when $\gamma = 0$, i.e., when there is no coupling between the electric and mechanical systems, the ground state has no excitations. However, this is no longer true when $|\gamma| > 0$ and $\omega_{\rm e} \neq \omega_{\rm m}$. By squeezing the zero-point fluctuations of the magnetomechanical system the ground state becomes entangled. Ground-state entanglement induces the emergence of negative energy-density regions in quantum systems [45]. The entanglement present when $\langle \hat{n}_{\rm m} + \hat{n}_{\rm e} \rangle > 0$ represents a signature of the quantum nature of the magnetomechanical system. This magnetomechanical

system presents an approach for the generation of negative energy-density which can be implemented in protocols of quantum energy teleportation [45].

V. NONEQUILIBRIUM SYSTEM

So far, we have described the magnetomechanical system in an isolated environment, i.e., in the absence of decoherence. In this section we consider a semiclassical description in the presence of decoherence channels $\Gamma_e, \Gamma_m \neq 0$ and the response of the mechanical system to thermal excitations. In Sec. V A we describe observable properties such as magnetomechanical damping and magnetomechanical frequency shift.

The simplest dynamics of the magnetomechanical system out of equilibrium arises when we consider the mechanical system to be in contact with a thermal bath through the decoherence channel $\Gamma_m \neq 0$. In this case we consider the external driving force $F_{ext}(t)$ no longer dominated by the Lorentz force $F_L(t)$ but by the random thermal Langevin force $F_{th}(t)$. The mechanical system is then driven by $F_{th}(t)$ and as a result it has a randomly time-varying amplitude and phase. In most experiments, the oscillations of microscale mechanical systems are analyzed as a noise spectrum in frequency space. Here we describe the stationary spectral properties of the magnetomechanical system and analyze the influence of the LC circuit on the mechanics.

The fluctuations of the mechanical displacement are a consequence of Brownian motion due to the fact that the mechanical oscillator is driven by a noisy thermal force. We describe the system using the Langevin equation $\partial \hat{O}/\partial t = (i/\hbar)[\hat{H}_L, \hat{O}] + \hat{\mathcal{N}}_{\mathcal{O}}$ for an arbitrary observable $\hat{O}$, where $\hat{\mathcal{N}}_{\mathcal{O}}$ represents the noise introduced by the interaction of the observable $\hat{O}$ with its environment. We calculate the Langevin equation for the coupled system of observables $\hat{z}$, $\hat{p}$, $\hat{q}$, and $\hat{\phi}$, which reads as

$$
\begin{aligned}
\dot{\hat{z}} &= \frac{\hat{p}}{m} + g_0 \sqrt{\frac{L}{m}} \hat{q}, \\
\dot{\hat{p}} &= m\omega_m^2 \hat{z} - \Gamma_m \hat{p} - \hat{F}_{ext}(t), \\
\dot{\hat{q}} &= \frac{\hat{\phi}}{L}, \\
\dot{\hat{\phi}} &= L\Omega_e^2 \hat{q} - \Gamma_e \hat{\phi} - g_0 \sqrt{\frac{L}{m}} \hat{p} + \hat{V}_{ext}(t).
\end{aligned}
\tag{26}
$$

It is clear that the noisy elements are introduced in the "momentum" terms as they are commonly associated to friction forces. From the experimental point of view, it is easier to measure the properties of the system in the frequency domain, looking at the stationary case. For the stationary case it's possible to consider that we measure continuously for a finite time τ; in this situation, the frequency components of the displacement are (and the definition is extended to all the other operators)

$$
\tilde{z}(\omega) = \frac{1}{\sqrt{\tau}} \int_0^\tau \hat{z}(t)e^{i\omega t}dt.
\tag{27}
$$

For the limit $\tau \to \infty$, the response of the mechanical oscillator to an external drive is $\tilde{z}(\omega) = \chi_m(\omega)\tilde{F}_{ext}(\omega)$, where the susceptibility of the mechanics is $\chi_m(\omega) = (m(\omega_m^2 - \omega^2 + i\omega\Gamma_m))^{-1}$.
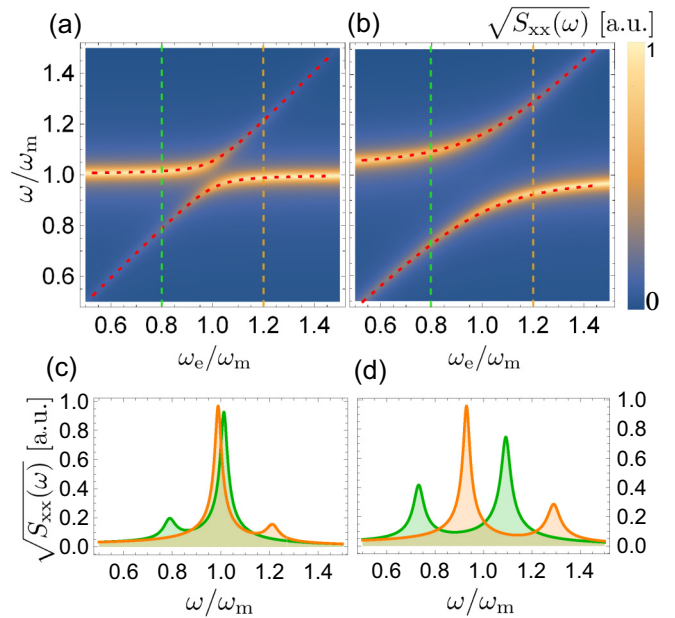

FIG. 4. (a) Plot of the position displacement $\sqrt{\langle |z|^2 \rangle} = \sqrt{S_{xx}(\omega)}$ [a.u.] considering the parameters $(\Gamma_m, \Gamma_e, g_0) = (0.025, 0.05, 0.1) \times \omega_m$ as a function of the frequency ω/ω_m and ω_e/ω_m, where we set $m = L = 1$. The normal mode frequencies $\Omega_\pm$ are shown as red dashed lines and avoided crossing is observed. For $\omega_e = 0.8\omega_m$ (green dashed line) and $\omega_e = 1.2\omega_m$ (orange dashed line) we show the profile in (c) which is normalized to the maximum. (b) Plot of the mechanical response considering the parameters $(\Gamma_m, \Gamma_e, g_0) = (0.025, 0.05, 0.3) \times \omega_m$ as a function of the frequency ω/ω_m and ω_e/ω_m. The normal mode frequencies $\Omega_\pm$ are shown as red dashed lines and avoided crossing is observed. For $\omega_e = 0.8\omega_m$ (green dashed line) and $\omega_e = 1.2\omega_m$ (orange dashed line) we show the profile in (d), which is normalized to the maximum.

In the regime where $g_0 > 0$, we calculate the expected value of the operators that we obtained from the Langevin equation and transformed into the frequency domain $\langle \tilde{z} \rangle$, $\langle \tilde{p} \rangle$, $\langle \tilde{q} \rangle$, and $\langle \tilde{\phi} \rangle$. One obtains a set of coupled equations represented in matrix form as $\mathbf{Y} = (\mathbf{R} + i\omega\mathbf{I})\mathbf{Y}$, which has normal mode frequencies,

$$
\Omega_\pm^2 = \tfrac{1}{2}\Xi^2 \pm \tfrac{1}{2}\sqrt{4g_0^2\omega_m^2 + \Xi^4 - 4\omega_m^2\Omega_e^2},
\tag{28}
$$

where $\Xi^2 = \omega_m^2 + \Omega_e^2 + \Gamma_e\Gamma_m$, the vector $\mathbf{Y} = (\langle \tilde{z} \rangle, \langle \tilde{p} \rangle, \langle \tilde{q} \rangle, \langle \tilde{\phi} \rangle)$, and

$$
\mathbf{R} = \begin{pmatrix}
0 & \frac{1}{m} & \sqrt{\frac{L}{m}}g_0 & 0 \\
-m\omega_m^2 & -\Gamma_m & 0 & 0 \\
0 & 0 & 0 & \frac{1}{L} \\
0 & -\sqrt{\frac{L}{m}}g_0 & -L\Omega_e^2 & -\Gamma_e
\end{pmatrix}.
\tag{29}
$$

The normal mode frequencies are shown in Figs. 4(a) and 4(b) as red dashed lines. The coupling g_0 is characterized experimentally by the splitting $\Omega_+ - \Omega_- \approx g_0$ in the power spectral density (PSD) [14]. If the splitting is observable, it is a signature of strong coupling between the modes. Below we find that strong coupling can be achieved in the linear regime of this magnetomechanical system.

A. Mechanical susceptibility

In a self contained fashion, the presence of the magnetomechanical coupling $g_0 > 0$ creates a "circulation" of energy. The mechanical displacement generates a voltage in the LC resonator, while this one generates a magnetic field that exerts a force on the mechanical resonator. Intuitively, it is clear that the coupling might modify the bare mechanical susceptibility $\chi(\omega)$. This modified mechanical susceptibility is now called the effective susceptibility $\chi_{\text{eff}}(\omega)$ and is obtained from the solution for the set of coupled equations **Y**. We can express $\chi_{\text{eff}}(\omega)$ in terms of the mechanical bare susceptibility plus a magnetomechanical modification $\Sigma(\omega)$ such that

$$\chi_{\text{eff}}(\omega) = \frac{1}{m(\omega_{\text{m}}^2 - \omega^2 + i\omega\Gamma_{\text{m}}) + \Sigma(\omega)}, \qquad (30)$$

where similar to optomechanics, $\Sigma(\omega)$ represents the so called self-energy [36]. The modification of the mechanical susceptibility can be classified into a magnetomechanical induced damping rate $\Gamma_{\text{mm}}(\omega) = -\text{Im}[\Sigma(\omega)]/m\omega$ and a magnetomechanical induced frequency shift $\delta\omega_{\text{m}}(\omega) = \text{Re}[\Sigma(\omega)]/2m\omega$. Explicitly, these parameters take the form of the magnetomechanical damping

$$\Gamma_{\text{mm}}(\omega) = -g_0^2 \left[\frac{\omega^2(\Gamma_{\text{e}} - \Gamma_{\text{m}}) + \Gamma_{\text{m}}\omega_{\text{e}}^2}{\Gamma_{\text{e}}^2\omega^2 + (\omega^2 - \omega_{\text{e}}^2)^2} \right] \qquad (31)$$

and magnetomechanical induced frequency shift

$$\delta\omega_{\text{m}}(\omega) = \frac{g_0^2\omega}{2} \left[\frac{\omega_{\text{e}}^2 - \omega^2 - \Gamma_{\text{e}}\Gamma_{\text{m}}}{\Gamma_{\text{e}}^2\omega^2 + (\omega^2 - \omega_{\text{e}}^2)^2} \right]. \qquad (32)$$

The control of parameters such as $\Gamma_{\text{mm}}(\omega)$ and $\delta\omega_{\text{m}}(\omega)$ make it possible to implement protocols such as cooling or heating of the mechanical oscillator through the LC resonator within this magnetomechanical approach.

B. Spectral properties

Commonly, the properties of the mechanical systems are experimentally characterized by measuring the power spectral density (PSD), which we define as

$$S_{\text{xx}}(\omega) = \langle |\tilde{z}(\omega)|^2 \rangle = \langle |\chi_{\text{eff}}(\omega)|^2 \tilde{F}_{\text{th}}(\omega) \rangle. \qquad (33)$$

The PSD has units of m^2/Hz and represents the distribution of energy in each frequency component of the signal [12]. In the case where the thermal energy drives the mechanical oscillation, it is possible to relate the variance of the amplitude of the oscillation to the thermal energy stored in the oscillator by the *fluctuation dissipation theorem* $\langle |\tilde{z}(\omega_{\text{m}})|^2 \rangle = k_B \, T \, \Gamma_{\text{eff}}(m\omega_{\text{m}})^{-1}$, where $\Gamma_{\text{eff}} = \Gamma_{\text{m}} + \Gamma_{\text{mm}}$. The amplitude of the oscillation is then related as $\sqrt{S_{\text{xx}}(\omega)} = \sqrt{\langle |\tilde{z}(\omega)|^2 \rangle}$. In Fig. 4(a) and Fig. 4(c) we plot $\sqrt{S_{\text{xx}}(\omega/\omega_{\text{m}})}$ with values $(\Gamma_{\text{m}}, \Gamma_{\text{e}}, g) = (0.025\omega_{\text{m}}, 0.05\omega_{\text{m}}, 0.1\omega_{\text{m}})$. In Figs. 4(b) and 4(d) the considered values are $(\Gamma_{\text{m}}, \Gamma_{\text{e}}, g) = (0.025\omega_{\text{m}}, 0.05\omega_{\text{m}}, 0.3\omega_{\text{m}})$. Figures 4(c) and 4(d) show two plots for $\tilde{z}(\omega)$ values of ω_{e}, in green $\omega_{\text{e}} = 0.8\omega_{\text{m}}$ and orange $\omega_{\text{e}} = 1.2\omega_{\text{m}}$. Normal mode splitting indicative of strong coupling might be observed with mechanical oscillators

with quality factor as low as $Q_{\text{m}} = \omega_{\text{m}}/\Gamma_{\text{m}} = 40$ for a system with the characteristics described in the next section.

The solution to the set of coupled equations **Y** also suggests that the mechanical response is modified in the presence of an external driving voltage on the circuit $\tilde{V}_{\text{ext}}(\omega)$. In a particular case, if the LC resonator is thermally driven $\tilde{V}_{\text{ext}}(\omega) = \tilde{V}_{\text{th}}(\omega)$, this thermal drive can be measured with the mechanics. The response of the mechanical resonator to an external thermal voltage depends on a mechanical-voltage susceptibility $\chi_{\text{V}}(\omega) = \chi_{\text{eff}}(\omega)\sqrt{\frac{m}{L}}\frac{g_0(\Gamma_{\text{m}} - i\omega)}{(i\Gamma_{\text{e}}\omega + \omega^2\omega_{\text{e}}^2)}$. The PSD of the mechanics due to excitation in the electronics is then

$$S_{\text{VV}}(\omega) = \langle |\chi_{\text{V}}(\omega)|^2 \tilde{V}_{\text{ext}}(\omega) \rangle. \qquad (34)$$

The mechanical response to an external force and an electric drive is

$$\tilde{z}(\omega) = \chi_{\text{eff}}(\omega)\tilde{F}_{\text{ext}}(\omega) + \chi_{\text{V}}(\omega)\tilde{V}_{\text{ext}}(\omega). \qquad (35)$$

The mechanical spectrum of Eq. (35) will provide a way to experimentally measure the response of the mechanical oscillator to external forces applied on itself and external voltages applied on the LC, as well as its coupling.

VI. MAGNETOMECHANICAL DEVICE

Up to this point, we have treated the magnetomechanical system in a general fashion. Here we describe a design feasible to fabricate with currently available photo and e-beam lithography techniques and materials. Here we describe some technical details regarding its fabrication and practical implementation. Our model considers the state-of-the-art experimental micro- and nanofabrication techniques. In this particular design we study mostly the influence on the coupling rate g_0 due to the geometry and factors such as the height of the magnet h_{m}, relative equilibrium vertical distance between the magnet and the coil u_0, number of turns of the inductor/coil N, and width w of the wire/separation. The magnetomechanical system is in principle able to achieve coupling rates g_0 that exceed the values of the mechanical resonance frequency ω_{m}, which is extremely challenging for optomechanical systems.

The successful implementation of our magnetomechanical system [Fig. 5(c)] requires a two-chip fabrication process, separated in two main steps. The first chip [Fig. 5(a)] consist of a double clamped mechanical resonator (Sec. VIA). The second chip [Fig. 5(b)] consists of a spiral coil and a planar capacitor fabricated on a sapphire substrate (Sec. VIB). Each one of the chips is individually fabricated and later joint flipping the top chip (mechanical resonator) and adjusting the separation between them. These flipped joint chips form a system similar to the state-of-the-art 3D cavities recently developed [46,47].

A. Mechanical system

In this section we describe the protocol for the microfabrication of the mechanical oscillator of the magnetomechanical system. The mechanical oscillator could be fabricated as a double clamped beam 10 μm long and 1 μm wide on a thin film Si_3N_4 membrane 100 nm thick on Si substrate. The membrane can be patterned using standard photolithography techniques; after exposure and development of the positive
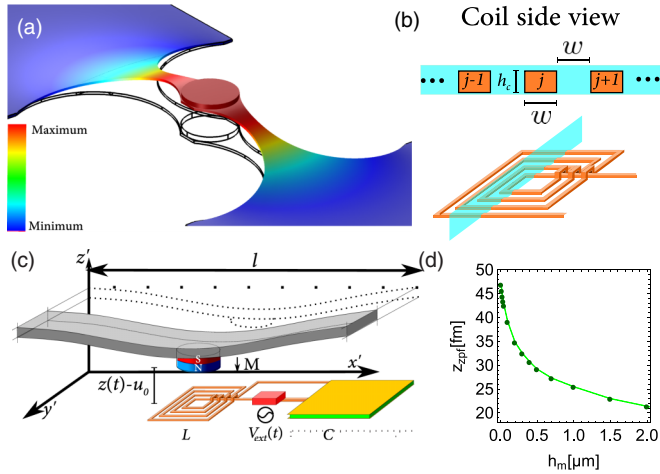
FIG. 5. (a) Diagram of the fundamental mechanical mode of a double clamped beam made out of a Si_3N_4 membrane smoothly etched. The membrane has a cylinder on top that represents the magnet. (b) Diagram of the coil on the electronic chip. In blue an axial plane cut showing the transversal area $w \times h_c$ of each wire of the coil. The width and spacing is w and h_c is the thickness of the wire. (c) Representation of the flipped chip approach that places the double clamped beam resonator above the electronic chip. (d) Plot of the zero point fluctuation z_{ZPF} for the fundamental mode as a function of the thickness/height of the magnet h_m.

FIG. 6. (a) Plot of ω_m as a function of h_m and m of the fundamental mode. (b) Determination of the ratio g_0/ω_m as a function of $\mathcal{T}$ for $h_m = 10$ nm, $h_m = 50$ nm, and $h_m = 200$ nm. The parameters considered here are $w = 100$ and $N = 2$ of the inductor. In red the thickest magnet of $h_m = 200$ nm. In orange the curve that corresponds to $h_m = 50$ nm. In purple, the curve that corresponds to $h_m = 10$ nm. (c) Estimation of g_0/ω_m as a function of w. In these results $h_m = 200$ nm, with the one, the oscillator has an effective mass $m = 9.9 \times 10^{-15}$ kg and a mechanical resonant frequency $\omega_m/2\pi = 3.2$ MHz. The gap considered in this result is $\mathcal{T} = 10$ nm. In blue, the curve corresponding to $N = 15$, in green $N = 10$, in red $N = 5$, and in orange $N = 2$. (d) Ratio g_0/ω_m as a function of N. The numerical values were calculated considering a cylindrical magnet with $h_m = 200$ nm, $\mathcal{T} = 10$ nm, and $w = 100$ nm. All the calculations were performed considering a magnetization $\mu_0|M| = 0.264$ T. The blue shaded regions represent the values that lay in the ultrastrong coupling regime.

photoresist the open regions are etched using *Reactive-Ion Etch* (RIE) fabrication technology. The finite element model (Comsol) in Fig. 5(a) shows the fundamental motional mode shape of the loaded double clamped beam made out of Si_3N_4. It has been reported that Si_3N_4 has exceptional mechanical properties under cryogenic conditions [48], which makes it suitable for future magnetomechanical setups. Mechanical oscillators made out of Si_3N_4 membranes have typical values for mechanical quality factor $Q_m = \omega_m/\Gamma_m = 10^5$.

On top of the patterned beam a second photolithographic step requires spin coating of a negative photoresist and exposing it with the magnet pattern. After the exposure and development of the pattern a thin film magnetic material is deposited, similar to the coating process for cantilever's AFM magnetized tips. The final step is the gentle release of the mechanical oscillator, which can be done using dry etch in a XeF_2 chamber for Si etch. This is an isotropic etch for Si which will remove the Si under the resonator. The thickness of the magnet h_m can be easily controlled during the deposition of the magnetic film. The cylindrical magnet is then formed at the center of the double clamped beam through lift-off of the negative resist. It is important to highlight that the remarkable mechanical properties of Si_3N_4 membranes remain largely unchanged when thin films are deposited on them [49] far from the clamping region. The magnetic flux from the magnet will determine the magnitude of the interaction as the coupling rate $g_0 \propto M$. It is desirable to have magnetic materials that support high density magnetization in thin films. A magnetic material with such characteristics and which has been extensively studied is Co-Fe, with a large number of different alloys [50]. Here we chose a standard one with density $\rho = 7.81$ g/cm^3 and a conservative value for the
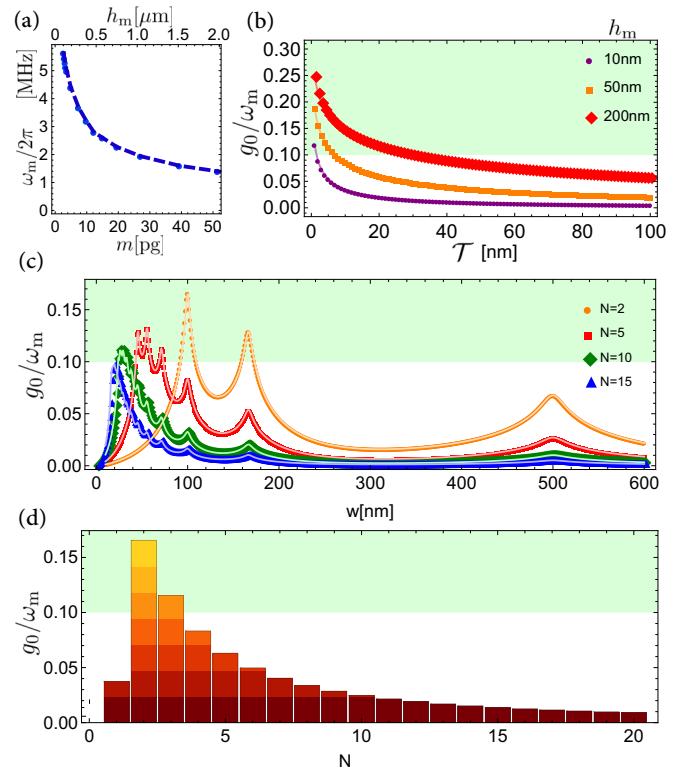
magnetization $\mu_0|\mathbf{M}| = 0.264$ T. Modern alloys have reached saturation magnetization up to $\mu_0|\mathbf{M}| = 2.4$ T [51]. The radius of the magnet is fixed to $r_m = 0.5$ μm and is a suitable size for photo or e-beam lithography; the only degree of freedom that we explore now is the height of the magnet h_m which is represented as the thickness of the magnetic thin film thickness. Considering the mass of the double clamped beam and the load of the magnet with its density, we calculate the effective mass m and the resonance frequency ω_m for the fundamental mechanical mode of the mechanical system as a function of h_m; it is shown in Fig. 6(a). By controlling the thickness of the deposited magnetic material, we can easily alter both ω_m, m also on the coupling rate g_0. In Fig. 5(d) we plot the zero point motion $z_{ZPF} = \sqrt{\frac{\hbar}{2m\omega_m}}$ as a function of the magnet thickness h_m. The control and tuning of the mechanical

frequency has two different limits. In one limit, films which are only a few nanometers thick will result in a higher frequency mechanical oscillator, making the interaction with the *LC* circuits technically more feasible. On the other hand, thicker films result in higher magnetic volumes and therefore stronger magnetic interactions.

B. Electrical circuit

The electronic component of the magnetomechanical system requires one to be fabricated on an individual chip. Following standard nanofabrication techniques for coils [15,52,53], the chip can be fabricated on a sapphire substrate placing the micro/nanofabricated coil depicted in Fig. 5(b), where a first layer of metal is deposited on the surface of the chip. Following a spin coating of e-beam resist (PMMA) for later exposure and patterning of the central electrode and the flat part of the spiral inductor, etching the metal through wet etch. A sacrificial layer of resist is deposited and then exposed to pattern the bridge, following an oxide removal of a few nm with Ar bombarding on the surface and the successive second layer of metal deposition to build the metallic bridge. A last step of resist removal either wet or dry needs to be implemented to remove the sacrificial layer.

A schematic representation of a spiral coil is shown in Fig. 5(b); we also show a transverse cut to define w as the packing parameter. The packing parameter represents the width of the wire but also the spacing between each one of the wires that make a single turn. The maximum resolution of a nanofabrication system will determine the minimum value for w.

C. Coupled system

The coupled magnetomechanical system requires a double chip packaging. This particular packaging resembles the on chip 3D-cavity implementations, taking the chip with the mechanical oscillator and flipping it over the second chip with the *LC* resonator as the scheme shows in Fig. 5(c).

Considering Eq. (3) and the initial separation u_0, we can numerically estimate the value g_0 as a function of several parameters, such as the gap between the edge of the magnet $\mathcal{T}$, the number of turns of the coil N, and the packing parameter w that represents the width and separation between the wires of the coil. The numerical results for the ratio of the coupling rate and the mechanical frequency g_0/ω_m as a function of three different parameters are shown in Figs. 6(a), 6(b), and 6(c). In Fig. 6(b) the ratio g_0/ω_m is presented as a function of the gap $\mathcal{T} = u_0 - h_m/2$ between the coil and the edge of the magnet, for different thickness of the magnet h_m and with $(N; w) = (2; 100 \text{ nm})$. It is observable that the same tendency is followed for different thickness of the magnetic film. As h_m and the magnetic volume increases, the maximum of the coupling rate achievable increases, but not linearly. Figure 6(b) shows a region in blue, where ratios of $g_0/\omega_m \approx 0.1$ lead to physics in the ultrastrong coupling regime. The importance of this result relies on the unexplored regime for mechanical systems. This regime has been recently observed in superconducting qubits [54]. Figure 6(c) shows numerical simulations of g_0/ω_m as a function of w with

parameters $(N; h_m; \omega_m) = (2; 200 \text{ nm}; 2\pi \times 3.2 \text{ MHz})$. For this calculation we considered a magnet with $h_m = 200$ nm that for the fundamental mode has associated an effective mass $m = 9.9 \times 10^{-15}$ kg and whose mechanical resonant frequency is $\omega_m/2\pi = 3.2$ MHz. This magnet is separated $\mathcal{T} = 10$ nm from the spiral coil.

We calculate the ratio g_0/ω_m as a function of w for different values of N. We observe that N is also an important parameter due to its contribution to the inductance L. The inductance L of the spiral square inductor was calculated with finite element methods software (Comsol) and compared with analytical expressions [55]. The two methods yielded similar results and thus we chose to use the analytical expressions for simplicity and accuracy. The last parameter discussed in this paper is the enhancement of the coupling rate g_0 due to the number of turns of the nanofabricated coil. In Fig. 6(d) we plot the coupling rate ratio g_0/ω_m as a function of N keeping the parameters $(\mathcal{T}; h_m; \omega_m) = (10 \text{ nm}; 200 \text{ nm}; 2\pi \times 3.2 \text{ MHz})$ fixed while maximizing over w. We observe that at $N = 2$ the maximum ratio is obtained due to the low inductance which favors the increase in the coupling. As it was described, with the coupling rate $g_0 \propto |\mathbf{M}|$, we have restricted our calculations to conservative magnetization values and consider that regimes such as deep-strong coupling can be achieved using modern alloys with larger magnetization.

VII. CONCLUSION

The magnetomechanical system that we have proposed in this work provides a suitable instrument to explore magnetomechanical dynamics in the strong coupling regime and beyond. Our study remains valid for a regime where $g_0/\omega_m > 1$ (deep strong coupling).

We have introduced physical effects such as magnetomechanical damping, or magnetomechanical frequency shift, that can be further explored and implemented on cooling protocols, state swap, and electronic readout of the mechanical system. The magnetomechanical system provides an interface for hybrid quantum protocols on the control of mechanical oscillators using electric circuits. The interaction $\sim \hat{p}\hat{q}$ represents an attractive option for the implementation of protocols to perform backaction evading measurements on mechanical oscillators via electronics. We also note that the Hamiltonian breaks time-reversal symmetry due to its linear dependence on the mechanical momentum. We consider that this particular feature could help to understand some of the physics of symmetries at the mesoscale. We estimated the number of excitations that populate the ground state and observe that the magnetomechanical system is intrinsically entangled in the regime of low phonon-photon occupation regime.

Considering the recent rapid progress in experimental techniques and fabrication processes such as photo and e-beam lithography, we consider that our magnetomechanical system is a feasible proposal to be fabricated. We predict that a very large coupling g_0 might be potentially achieved. This large coupling facilitates the implementation of already existing optomechanical protocols such as manipulation, control, or cooling.

APPENDIX: MAGNETOMECHANICAL BREAK OF TIME REVERSAL SYMMETRY

The magnetomechanical system that we have introduced in this paper provides a diverse variety of interesting directions to explore quantum features for mechanical systems at the mesoscale. The linear character of the momentum coupling also represents an interesting framework to study the breaking of time-reversal symmetry in this hybrid electromechanical interface.

In quantum mechanics, time-reversal symmetry is a bijective mapping of the Hilbert space. This mapping is symmetric if and only if it leaves all the observable probabilities invariant. As we show below, the magnetomechanical linear Hamiltonian (14) is not invariant under time reversal. The time-reversal symmetry breaking phenomenon is a rare effect, which has been observed in circuit QED [56] but to our best knowledge it has not been observed in mechanical systems.

Following the definition for time-reversal symmetry we analyze $\hat{H}_L$, which is symmetric if and only if for a time-reversal operator $\hat{\Theta}$, there exists a phase $\vartheta(\hat{z})$, such that $\hat{H}_L = \hat{\Theta}\hat{H}_L\hat{\Theta}^{-1}$ is satisfied [56]. The most relevant properties described by Koch *et al.* [56] show that the operator $\hat{\Theta}$ acting on an eigenstate of the position $|\hat{z}\rangle$ leaves it invariant, but add

a phase $\Theta|\hat{z}\rangle = e^{i\vartheta(\hat{z})}|\hat{z}\rangle$ and the eigenstates of the position are time-reversal symmetric $\hat{\Theta}\hat{z}\hat{\Theta}^{-1} = \hat{z}$. Under the same time-reversal transformation $\hat{\Theta}$, the momentum is reflected and the gradient of a phase is added: $\hat{\Theta}\hat{p}\hat{\Theta}^{-1} = -\hat{p} + \nabla\vartheta(\hat{z})$. The selection of the phase $\vartheta(\hat{z})$ is determined by the gauge choice $\varphi(z)$ discussed in Eq. (6). We apply the time-reversal operator and obtain the transformed Hamiltonian, which reads as

$$\hat{\Theta}\hat{H}_L\hat{\Theta}^{-1} = \frac{1}{2m}(-\hat{p} + \sqrt{Lm}\,g_0\hat{q} + \nabla\vartheta(\hat{z}))^2$$
$$+ \omega_m^2\frac{m\hat{z}^2}{2} + \frac{\hat{\phi}^2}{2L} + \omega_e^2\frac{L\hat{q}^2}{2}. \qquad (A1)$$

The condition $\hat{H}_L = \hat{\Theta}\hat{H}_L\hat{\Theta}^{-1}$ to identify this system as time-reversal symmetric implies that a solution is given by $\nabla\vartheta(\hat{z}) = -2g_0\sqrt{Lm}\hat{q}$. In the particular case when the coupling is absent $g_0 = 0$ the solution to this condition is satisfied and the Hamiltonian satisfies the time-reversal symmetry $\hat{H}_L = \hat{\Theta}\hat{H}_L\hat{\Theta}^{-1}$. In any other case $g_0 \neq 0$ Eq. (6) suggests that the gauge choice is related to an electromagnetic auxiliary field $\mathbf{A} = \nabla\varphi(\hat{z})$; therefore, it must satisfy $\nabla \times \mathbf{A} = \mathbf{0}$, which in the presence of a magnetic field clearly contradicts $\mathbf{B} = \nabla \times \mathbf{A}$.

Summarizing, the magnetomechanical system described in this paper satisfies time-reversal symmetry in the absence of coupling, but breaks it when the linear magnetomechanical coupling is present. We want to highlight this property for the magnetomechanical system as an alternative to explore time-reversal symmetry breaking for mechanical systems.

[1] R. W. Andrews, R. W. Peterson, T. P. Purdy, K. Cicak, R. W. Simmonds, C. A. Regal, and K. Lehnert, Nat. Phys. **10**, 321 (2014).

[2] T. Bagci, A. Simonsen, S. Schmid, L. G. Villanueva, E. Zeuthen, J. Appel, J. M. Taylor, A. Sørensen, K. Usami, A. Schliesser *et al.*, Nature (London) **507**, 81 (2014).

[3] C. M. Caves, K. S. Thorne, R. W. Drever, V. D. Sandberg, and M. Zimmermann, Rev. Mod. Phys. **52**, 341 (1980).

[4] W. Marshall, C. Simon, R. Penrose, and D. Bouwmeester, Phys. Rev. Lett. **91**, 130401 (2003).

[5] I. Pikovski, M. R. Vanner, M. Aspelmeyer, M. S. Kim, and Č. Brukner, Nat. Phys. **8**, 393 (2012).

[6] T. Carmon, H. Rokhsari, L. Yang, T. J. Kippenberg, and K. J. Vahala, Phys. Rev. Lett. **94**, 223902 (2005).

[7] T. A. Palomaki, J. D. Teufel, R. W. Simmonds, and K. W. Lehnert, Science **342**, 710 (2013).

[8] L. A. De Lorenzo and K. C. Schwab, New J. Phys. **16**, 113020 (2014).

[9] G. I. Harris, D. L. McAuslan, E. Sheridan, Y. Sachkou, C. Baker, and W. P. Bowen, Nat. Phys. **12**, 788 (2016).

[10] M. Eichenfield, J. Chan, R. M. Camacho, K. J. Vahala, and O. Painter, Nature (London) **462**, 78 (2009).

[11] D. L. McAuslan, G. I. Harris, C. Baker, Y. Sachkou, X. He, E. Sheridan, and W. P. Bowen, Phys. Rev. X **6**, 021012 (2016).

[12] W. P. Bowen and G. J. Milburn, *Quantum Optomechanics* (CRC Press, Boca Raton, FL, 2015).

[13] A. D. OConnell, M. Hofheinz, M. Ansmann, R. C. Bialczak, M. Lenander, E. Lucero, M. Neeley, D. Sank, H. Wang, M. Weides *et al.*, Nature (London) **464**, 697 (2010).

[14] S. Gröblacher, K. Hammerer, M. R. Vanner, and M. Aspelmeyer, Nature (London) **460**, 724 (2009).

[15] J. D. Teufel, T. Donner, D. Li, J. W. Harlow, M. S. Allman, K. Cicak, A. J. Sirois, J. D. Whittaker, K. W. Lehnert, and R. W. Simmonds, Nature (London) **475**, 359 (2011).

[16] D. Hu, S.-Y. Huang, J.-Q. Liao, L. Tian, and H.-S. Goan, Phys. Rev. A **91**, 013812 (2015).

[17] A. A. Anappara, S. De Liberato, A. Tredicucci, C. Ciuti, G. Biasiol, L. Sorba, and F. Beltram, Phys. Rev. B **79**, 201303 (2009).

[18] D. Z. Rossatto, C. J. Villas-Bôas, M. Sanz, and E. Solano, Phys. Rev. A **96**, 013849 (2017).

[19] T. Holz, R. Betzholz, and M. Bienert, Phys. Rev. A **92**, 043822 (2015).

[20] D. Z. Rossatto, S. Felicetti, H. Eneriz, E. Rico, M. Sanz, and E. Solano, Phys. Rev. B **93**, 094514 (2016).

[21] N. Ares, T. Pei, A. Mavalankar, M. Mergenthaler, J. H. Warner, G. A. D. Briggs, and E. A. Laird, Phys. Rev. Lett. **117**, 170801 (2016).

[22] O. Romero-Isart, L. Clemente, C. Navau, A. Sanchez, and J. I. Cirac, Phys. Rev. Lett. **109**, 147205 (2012).

[23] M. Cirio, G. K. Brennen, and J. Twamley, Phys. Rev. Lett. **109**, 147206 (2012).

[24] G. Via, G. Kirchmair, and O. Romero-Isart, Phys. Rev. Lett. **114**, 143602 (2015).

[25] K. Xia, M. R. Vanner, and J. Twamley, Sci. Rep. **4**, 5571 (2014).

[26] P. Rabl, P. Cappellaro, M. V. G. Dutt, L. Jiang, J. R. Maze, and M. D. Lukin, Phys. Rev. B **79**, 041302(R) (2009).

[27] R. Ravaud, G. Lemarquand, S. Babic, V. Lemarquand, and C. Akyel, IEEE Trans. Magn. **46**, 3585 (2010).

[28] E. Benedetto, Afrika Matematika **28**, 23 (2017).

[29] C. K. Law, Phys. Rev. A **51**, 2537 (1995).

[30] Y.-D. Wang, K. Semba, and H. Yamaguchi, New J. Phys. **10**, 043015 (2008).

[31] J. C. Sankey, C. Yang, B. M. Zwickl, A. M. Jayich, and J. G. Harris, Nat. Phys. **6**, 707 (2010).

[32] A. Szorkovszky, A. A. Clerk, A. C. Doherty, and W. P. Bowen, New J. Phys. **16**, 043023 (2014).

[33] B. Levitan, A. Metelmann, and A. Clerk, New J. Phys. **18**, 093014 (2016).

[34] G. A. Brawley, M. R. Vanner, P. E. Larsen, S. Schmid, A. Boisen, and W. Bowen, Nat. Commun. **7**, 10988 (2016).

[35] M. Bienert and P. Barberis-Blostein, Phys. Rev. A **91**, 023818 (2015).

[36] M. Aspelmeyer, T. J. Kippenberg, and F. Marquardt, Rev. Mod. Phys. **86**, 1391 (2014).

[37] M. Aspelmeyer, S. Gröblacher, K. Hammerer, and N. Kiesel, JOSA B **27**, A189 (2010).

[38] S. Felicetti, M. Sanz, L. Lamata, G. Romero, G. Johansson, P. Delsing, and E. Solano, Phys. Rev. Lett. **113**, 093602 (2014).

[39] J. Bourassa, J. M. Gambetta, A. A. Abdumalikov, Jr., O. Astafiev, Y. Nakamura, and A. Blais, Phys. Rev. A **80**, 032109 (2009).

[40] J. Casanova, G. Romero, I. Lizuain, J. J. García-Ripoll, and E. Solano, Phys. Rev. Lett. **105**, 263603 (2010).

[41] P. Forn-Díaz, J. Lisenfeld, D. Marcos, J. J. García-Ripoll, E. Solano, C. J. P. M. Harmans, and J. E. Mooij, Phys. Rev. Lett. **105**, 237001 (2010).

[42] T. Niemczyk, F. Deppe, H. Huebl, E. P. Menzel, F. Hocke, M. J. Schwarz, J. J. Garcia-Ripoll, D. Zueco, T. Hümmer, E. Solano *et al.*, Nat. Phys. **6**, 772 (2010).

[43] J. Hausinger and M. Grifoni, Phys. Rev. A **82**, 062320 (2010).

[44] F. Hong-Yi and Y. Peng, Commun. Theor. Phys. **48**, 428 (2007).

[45] M. Hotta, *International Conference on Quantum Comunication and Quantum Networking* (Springer, New York, 2009), pp. 66–73.

[46] M. Yuan, V. Singh, Y. M. Blanter, and G. A. Steele, Nat. Commun. **6**, 8491 (2015).

[47] A. Noguchi, R. Yamazaki, M. Ataka, H. Fujita, Y. Tabuchi, T. Ishikawa, K. Usami, and Y. Nakamura, New J. Phys. **18**, 103036 (2016).

[48] T. P. Purdy, R. W. Peterson, P. L. Yu, and C. A. Regal, New J. Phys. **14**, 115021 (2012).

[49] P.-L. Yu, T. P. Purdy, and C. A. Regal, Phys. Rev. Lett. **108**, 083603 (2012).

[50] P. Dorsey, P. Lubitz, D. Chrisey, and J. Horwitz, J. Appl. Phys. **79**, 6338 (1996).

[51] Y. Fu, X. Cheng, and Z. Yang, Phys. Status Solidi A **202**, 1150 (2005).

[52] E. E. Wollman, C. U. Lei, A. J. Weinstein, J. Suh, A. Kronwald, F. Marquardt, A. A. Clerk, and K. Schwab, Science **349**, 952 (2015).

[53] P. B. Dieterle, M. Kalaee, J. M. Fink, and O. Painter, Phys. Rev. Appl. **6**, 014013 (2016).

[54] F. Yoshihara, T. Fuse, S. Ashhab, K. Kakuyanagi, S. Saito, and K. Semba, Nat. Phys. **13**, 44 (2017).

[55] S. S. Mohan, M. del Mar Hershenson, S. P. Boyd, and T. H. Lee, IEEE J. Solid-State Circuits **34**, 1419 (1999).

[56] J. Koch, A. A. Houck, K. L. Hur, and S. M. Girvin, Phys. Rev. A **82**, 043811 (2010).